ROYAL SOCIETY OF CHEMISTRY

PAPER

Check for updates

Influence of modification of Ti₃C₂ MXene with ceramic oxide and noble metal nanoparticles on its antimicrobial properties and ecotoxicity towards selected algae and higher plants†

A. Rozmysłowska-Wojciechowska,[*a] E. Karwowska,[b] S. Poźniak,[a] T. Wojciechowski,[c] L. Chlubny,[d] A. Olszyna,[a] W. Ziemkowska[c] and A. M. Jastrzębska [ID] [*a]

The number of investigations regarding the application of 2D nanosheets of MXenes in different technological areas is growing rapidly. Different surface modifications of MXenes have been introduced to date in order to tailor their properties. As a result, surface-modified MXenes could be released in the environment from filtration membranes, adsorbents, or photocatalysts. On the other hand, assessment of their environmental impact is practically unexplored. In the present study, we examined how modification of the antimicrobial Ti₃C₂ MXene with ceramic oxide and noble metal nanoparticles affects its toxic behavior. The expanded 2D sheets of the Ti₃C₂ MXene phase were modified with Al₂O₃/Ag, SiO₂/Ag, and SiO₂/Pd nanoparticles using the sol–gel method and extensively characterized. The obtained 2D nanocomposite structures were characterized by antibacterial properties. The ecotoxicological assays considered green algae (*Desmodesmus quadricauda*) as well as two higher plants: sorghum (*Sorghum saccharatum*) and charlock (*Sinapis alba*). Our results revealed that obtained nanomaterials can cause both stimulating and inhibiting effects towards algae, and the ecotoxicity depended on the concentration and the type of modification. The study reveals the intriguing property of pristine Ti₃C₂ which highly stimulated green algae growth at low concentrations. It also shows that modification of pristine Ti₃C₂ MXene with different nanoparticles changes the ecotoxicological effects of the resulting nanocomposite 2D structures. We have also indicated nanocomposite structures that does not revealed the toxic effect on tested organisms *i.e.* the Ti₃C₂ MXene surface-modified with Al₂O₃/Ag was not phyto- and eco-toxic. This work helps with better understanding of the reactivity of surface-modified MXenes towards chosen organisms, giving more information concerning the potential impact of tested nanocomposites on the ecosystems.

1. Introduction

The number of investigations regarding the application of 2D nanosheets of MXenes in different technological areas is growing rapidly. The term 'MXene' reflects the stoichiometry of the material *i.e.* $M_{n+1}X_n$, in which M stands for early transition metal, X relates to carbon or nitrogen, while $n = 1$, 2 or 3. MXenes are obtained from their parent MAX phases, caused by expansion in concentrated HF which removes the A atom a metal from group 13 or 14 of the periodic table. MXenes are simply chemically expanded structures of MAX phases and are known as early transition metal carbides and nitrides.[2] Their attractive properties have allowed several applications, including filtration membranes,[3] adsorbents,[4] photocatalysts,[4] and antimicrobials.[5] It should be noted, however, that the potential toxicity of MXenes towards the natural environment has been practically unexplored. So far, the only publication in this area is Nasrallah *et al.*,[1] who reported the lack of significant toxicity of the pristine Ti₃C₂ MXene towards zebrafish embryos especially that Ti₃C₂ possess antimicrobial properties[5,6] contrary to *e.g.* Ti₂C MXene.[7,8] Many studies have considered different modifications of MXenes' surfaces, which were carried out in order to tailor their specific chemical activities. The surface-modifications with nanoparticles that have been

ᵃWarsaw University of Technology, Faculty of Materials Science and Engineering, Woloska 141, 02-507 Warsaw, Poland. E-mail: anita.rozmyslowska@gmail.com; szymonpozniak0@gmail.com; aolszyna@meil.pw.edu.pl; agsolgala@gmail.com; Fax: +48-22-234-57-19; Tel: +48-22-234-74-49

ᵇWarsaw University of Technology, Faculty of Building Services, Hydro and Environmental Engineering, Nowowiejska 20, 00-653 Warsaw, Poland. E-mail: ewa.karwowska@pw.edu.pl

ᶜWarsaw University of Technology, Faculty of Chemistry, Noakowskiego 3, 00-664 Warsaw, Poland. E-mail: twojciechowski@ch.pw.edu.pl; ziemk@ch.pw.edu.pl

ᵈAGH University of Science and Technology, Faculty of Materials Science and Ceramics, Mickiewicza 30, 30-059 Krakow, Poland. E-mail: leszek@agh.edu.pl

introduced for MXenes include: SnO_2,[9,10] TiO_2,[11–18] Nb_2O_5,[13] Cu_2O,[19,20] Rh,[21] Ru,[22] bimetallic Ru/Ni[23] or Co/Ni,[24] Mn_3O_4,[25] MnO_2,[26] Sb_2O_3,[27] NiO_2,[28] the transition metals Fe, Co, and Ni,[29] and Ni/Al hydroxide.[30] Additionally, some interesting antimicrobial 2D heterostructures based on Ti_3C_2 MXene were also prepared.[31] At the same time, some concerns have been raised about the effects if such nanocomposite 2D systems were released into the environment. The effective method of overcoming this problem is to use the surface-modification. It enables sophisticated managing of the biological activity of 2D materials. It was previously shown, that modification of the surface of 2D materials with ceramic/noble metal nanoparticles has large impact on material properties in terms of biocidal action.[32,33] Also, changing type of noble metal in *e.g.* TiO_2/M nanocomposites changes toxicity of the material.[34] Additionally, changing TiO_2 to Al_2O_3, SiO_2 or ZnO_2 in the Me_xO_y/Ag can shift the toxicity from one particular bacteria strain towards another.

In the present study, for the first time, we examine how modification of the antimicrobial Ti_3C_2 MXene with ceramic oxide and noble metal nanoparticles affects its ecotoxic behavior. In our ecotoxicological studies with nanocomposites: Ti_3C_2/3% Al_2O_3/2% Ag, Ti_3C_2/3% SiO_2/2% Ag, and Ti_3C_2/3% SiO_2/2% Pd we have chosen the green algae (*Desmodesmus quadricauda*) and two species of higher plants: sorghum (*Sorghum saccharatum*) and charlock (*Sinapis alba*). All of them are representatives of the primary producers – the first level of the matter circulation and a food chain in the ecosystems. This study will be suitable for a better understanding of the impact of surface-modified MXenes in the organisms belonging to the group playing the essential role in the production of organic matter in ecosystems and in consequence make it easier to estimate the potential impact of tested nanocomposites on the natural environment.

2. Experimental

2.1. Synthesis procedure of the Ti_3C_2 MXene modified with SiO_2, Al_2O_3, Ag and Pd nanoparticles

The materials examined for ecotoxicity and phytotoxicity were: Ti_3C_2 MXene (used here as a reference sample) as well as nanocomposites of Ti_3C_2/3% Al_2O_3/2% Ag, Ti_3C_2/3% SiO_2/2% Ag, and Ti_3C_2/3% SiO_2/2% Pd.

The layered Ti_3AlC_2 MAX phase was synthesized using the SHS technique with a local ignition system.[35] Briefly, the SHS derived Ti_3Al powder, graphite powder (Merck no. 1.04206.9050, 99.8% pure, grain size 99.5% < 50 μm) were reacted in stoichiometric proportions, placed in the reactor and ignited for 60 seconds until end of the SHS process. The cooled product was immersed in dry isopropanol and grinded with WC balls in a rotary-vibratory mill for 8 hours. The dried Ti_3AlC_2 powder was then immersed in 48% hydrofluoric acid for 24 h at room temperature. About 10 cm³ of hydrofluoric acid was used per 1 g of the starting material. The resulting suspension was washed four times with deionized water and four times with technical grade ethanol. The solid product, layered Ti_2C, was dried overnight at room temperature.

The expanded 2D sheets of Ti_3C_2 MXene phase were modified with Al_2O_3, SiO_2, Ag, and Pd nanoparticles using the sol–gel method. The 2D nanocomposite of Ti_3C_2/3% Al_2O_3/2% Ag was prepared as follows: to a stirred suspension of Ti_3C_2 MXene (1.00 g), 1 cm³ of iso-propanol (Avantor, Bytom, Poland), 0.120 g of $Al(O^iPr)_3$, 0.036 g of silver lactate (as a precursor of Ag_2O), and 0.5 cm³ of distilled water were added. The reaction mixture was stirred in an open beaker until the volatiles evaporated (about 2 days).

2D nanocomposites of Ti_3C_2/3% SiO_2/2% Ag and Ti_3C_2/3% SiO_2/2% Pd were prepared as follows: to a stirred suspension of Ti_3C_2 MXene (1.00 g), 1 cm³ of iso-propanol, 0.094 g of $Si(OEt)_4$, precursors of Ag_2O or PdO nanoparticles (0.036 g of silver lactate or 0.053 g of palladium acetate, respectively), and 0.5 cm³ of distilled water were added. The reaction mixtures were stirred in open beakers until the volatiles evaporated (about 2 days). All reagents were obtained from Sigma-Aldrich (Poznań, Poland) and were used as delivered. The composition of the nanomaterials was determined assuming the purity of the Ti_3C_2 to be 100%.

2.2. Characterization of the morphology and structure of the obtained nanocomposite structures

The morphologies of the surface of Ti_3C_2 MXene, Ti_3C_2/Al_2O_3/Ag, Ti_3C_2/SiO_2/Ag, and Ti_3C_2/SiO_2/Pd nanocomposites were analyzed using scanning electron microscopy (SEM). The samples were directly deposited onto sticky carbon tape and coated with a carbon layer using a BAL-TEC SCD 005 sputter coater. Samples were subjected to morphology analysis with a LEO 1530 (Zeiss, USA) microscope, at an accelerating voltage of 2.0 kV.

The elemental composition was analyzed using an energy dispersive X-ray spectroscopy (EDS) unit coupled with a scanning electron microscope. The analysis gave information on the presence of specific elements in a chosen region of the sample.

The chemical compositions of the surfaces of Ti_3C_2 MXene, Ti_3C_2/Al_2O_3/Ag, Ti_3C_2/SiO_2/Ag, and Ti_3C_2/SiO_2/Pd nanocomposites were characterized using X-ray photoelectron spectroscopy (XPS). X-ray photoelectron spectroscopic measurements were performed using a PHI 5000 VersaProbe (ULVAC-PHI) spectrometer with monochromatic Al Kα radiation ($hv = 1486.6$ eV) from an X-ray source operating at 100 μm spot size, 25 W, and 15 kV. The high-resolution (HR) XPS spectra were collected with the hemispherical analyzer at a pass energy of 117.4 and an energy step size of 0.1 eV. The X-ray beam was incident at the sample surface at an angle of 45° with respect to the surface normal, and the analyzer axis was located at 45° with respect to the surface. Casa XPS software (version 2.3.18) was used to evaluate the XPS data. Deconvolution of all HR XPS spectra were performed using a Shirley background and a Gaussian peak shape with 30% Lorentzian character.

2.3. Analysis of physical properties and porous structure

The physical properties and porous structure of Ti_3C_2 MXene, Ti_3C_2/Al_2O_3/Ag, Ti_3C_2/SiO_2/Ag, and Ti_3C_2/SiO_2/Pd nanocomposites were analyzed using physical nitrogen sorption

isotherms. The preparation of samples included degassing under vacuum at a temperature of 300 °C for 24 hours. Physical nitrogen sorption isotherms were measured experimentally in a liquid nitrogen bath (−195.8 °C) using Quadrasorb-SI equipment (Quantachrome Instruments, USA). The specific surface area, S_{BET}, was determined using the Brunauer, Emmett, and Teller method (BET). The total pore volume, V_{pores}, and the surface area occupied by the pores, S_{pores}, were determined using the Barrett, Joyner, and Halenda method (BJH). The distributions of the pore sizes were further used for estimating the average pore size, D_{BJH}.

2.4. Analysis of antimicrobial properties

The bioactivities of Ti_3C_2 MXene, $Ti_3C_2/Al_2O_3/Ag$, $Ti_3C_2/SiO_2/Ag$, and $Ti_3C_2/SiO_2/Pd$ nanocomposites were analyzed qualitatively by an agar diffusion method using selected strains of both Gram-negative (*Escherichia coli*) and Gram-positive bacteria (*Bacillus* sp., *Staphylococcus aureus*, and *Sarcina lutea*), from the private collection of the Biology Department, Faculty of Building Services, Hydro and Environmental Engineering, Warsaw University of Technology.

In the diffusion method, microorganisms were spread in a line on the surface of a solid nutritive culture medium (Nutrient LAB-AGAR™, Biocorp) in Petri dishes. The samples of nanocomposites were subsequently placed on the surface of the bacterial inoculation. The prepared bacterial cultures were then incubated for 48 h at 26 °C (*Bacillus* sp. and *Sarcina lutea*) or 37 °C (*Escherichia coli* and *Staphylococcus aureus*). After incubation, the cultures were photographed, and the growth inhibition zones around the nanocomposite samples were measured. The size of the inhibition zone 2 mm and below was estimated as moderate inhibition (+) and the inhibition exceeding 2 mm was stated as the effective one (++). Five parallel measurements were accomplished and the final result was given as the average.

In order to estimate the antibacterial effect against a potentially pathogenic microorganisms, the additional quantitative analysis of the nanocomposites' bioactivity was accomplished with *Staphylococcus aureus*, using a dilution method. The test was carried out in nutrient broth medium (Biocorp), diluted 1 : 1 with the nanocomposite suspension, giving final nanocomponent concentrations from 0 mg l^{-1} (control sample) to 500 mg l^{-1}. The cultures were incubated at 37 °C for 24 hours. After the incubation, the optical density of the culture was measured in a spectrophotometer at a wavelength of 610 nm.

2.5. Analysis of ecotoxicity towards green algae

The ecotoxicity of Ti_3C_2 MXene, $Ti_3C_2/Al_2O_3/Ag$, $Ti_3C_2/SiO_2/Ag$, and $Ti_3C_2/SiO_2/Pd$ nanocomposites was tested using the green algae *Desmodesmus quadricauda*, which are organisms commonly used in ecotoxicological tests. The *D. quadricauda* cultures were grown at room temperature under continuous artificial lighting. The algal cultures were carried out in cameras recommended for standardized ALGAL TOXKIT test, in the Jankowski L5 growth medium, containing KNO_3 – 0.1 g l^{-1}, $Ca(NO_3)_2$ – 0.1 g l^{-1}, KH_2PO_4 – 0.04 g l^{-1}, $MgSO_4 \cdot 7H_2O$ – 0.03 g

l^{-1}, citric acid – 0.003 g l^{-1}, ferric citrate – 0.003 g l^{-1}, distilled water – 1000 ml, and supplied with 1 ml l^{-1} of a microelements solution (H_3BO_3 – 2.86 g l^{-1}, $MnCl_2 \cdot 7H_2O$ – 1.81 g l^{-1}, $ZnSO_4 \cdot 7H_2O$ – 0.222 g l^{-1}, MoO_3 – 0.176 g l^{-1}, NH_4VO_3 – 0.23 g l^{-1}, $CuSO_4 \cdot 7H_2O$ – 0.01 g l^{-1}, and $Co(NO_3)_2 \cdot H_2O$ – 0.02 g l^{-1}). The test was carried out at nanocomposite concentrations from 12.5 mg l^{-1} to 100 mg l^{-1}. The nanocomposite suspension was prepared by sonication. Two parallel series of algal cultures were grown for each concentration of the nanopowders; the results were presented as the average values of both experimental series. The number of algal cells was determined by direct counting under a light microscope, at the beginning of the experiment and after 7 days. The algal culture without nanocomposites was used as a control sample.

2.6. Analysis of phytotoxicity

In the present study, the phytotoxicity of Ti_3C_2 MXene, $Ti_3C_2/Al_2O_3/Ag$, $Ti_3C_2/SiO_2/Ag$, and $Ti_3C_2/SiO_2/Pd$ nanocomposites was evaluated using a standardized PHYTOTOXKIT set (Micro-BioTests, Sterling, VA), allowing to estimate the intensity of germination and root growth according to the ISO Standard 11269-1.32. The PHYTOTOXKIT also permits a preliminarily assessment of the condition of the plant seedlings during the experiments, based on the estimation of the growth of the sprout and its morphology at an early stage of plant growth. The test was carried out using the seeds of two species of plants, sorghum (*Sorghum saccharatum*) and charlock (*Sinapis alba*), in an artificial soil analogous to that recommended by the OECD for soil toxicity tests. The tests were conducted at two nanocomposite concentrations, 100 and 200 mg kg^{-1} of soil. The control was the same soil without any nanocomposite. After 3 days of cultivation at 26 °C, the germination intensity, the length of the sprout and roots, and the intensity of growth of the root system were determined. The results were documented photographically and interpreted using ImageJ software.

3. Results and discussion

The morphologies of Ti_3C_2 MXene, $Ti_3C_2/Al_2O_3/Ag$, $Ti_3C_2/SiO_2/Ag$, and $Ti_3C_2/SiO_2/Pd$ nanocomposites were examined using a scanning electron microscope (SEM) and are presented in Fig. 1. The typical expanded structure of Ti_3C_2 MXene (Fig. 1a), *i.e.* the nano-sized sheets with the slit-shaped pores, can clearly be seen. The Ti_3C_2 structure was then surface-modified with composite nanoparticles of Al_2O_3/Ag (Fig. 1b), SiO_2/Ag (Fig. 1c), and SiO_2/Pd (Fig. 1d). The SEM observations also indicated that the sizes of the composite nanoparticles varied and were generally below 100 nm, which confirmed the formation of nanocomposite systems.

EDS analyses of the $Ti_3C_2/Al_2O_3/Ag$, $Ti_3C_2/SiO_2/Ag$, and $Ti_3C_2/SiO_2/Pd$ nanocomposites are presented in Fig. 2 and show signals associated with the presence of C, Ti, O, and F that are similar for all samples. Additionally, the presence of signals related to Ag confirmed the presence of silver in $Ti_3C_2/Al_2O_3/Ag$ (Fig. 2b) and $Ti_3C_2/SiO_2/Ag$ (Fig. 2c). Also, for the $Ti_3C_2/SiO_2/Pd$
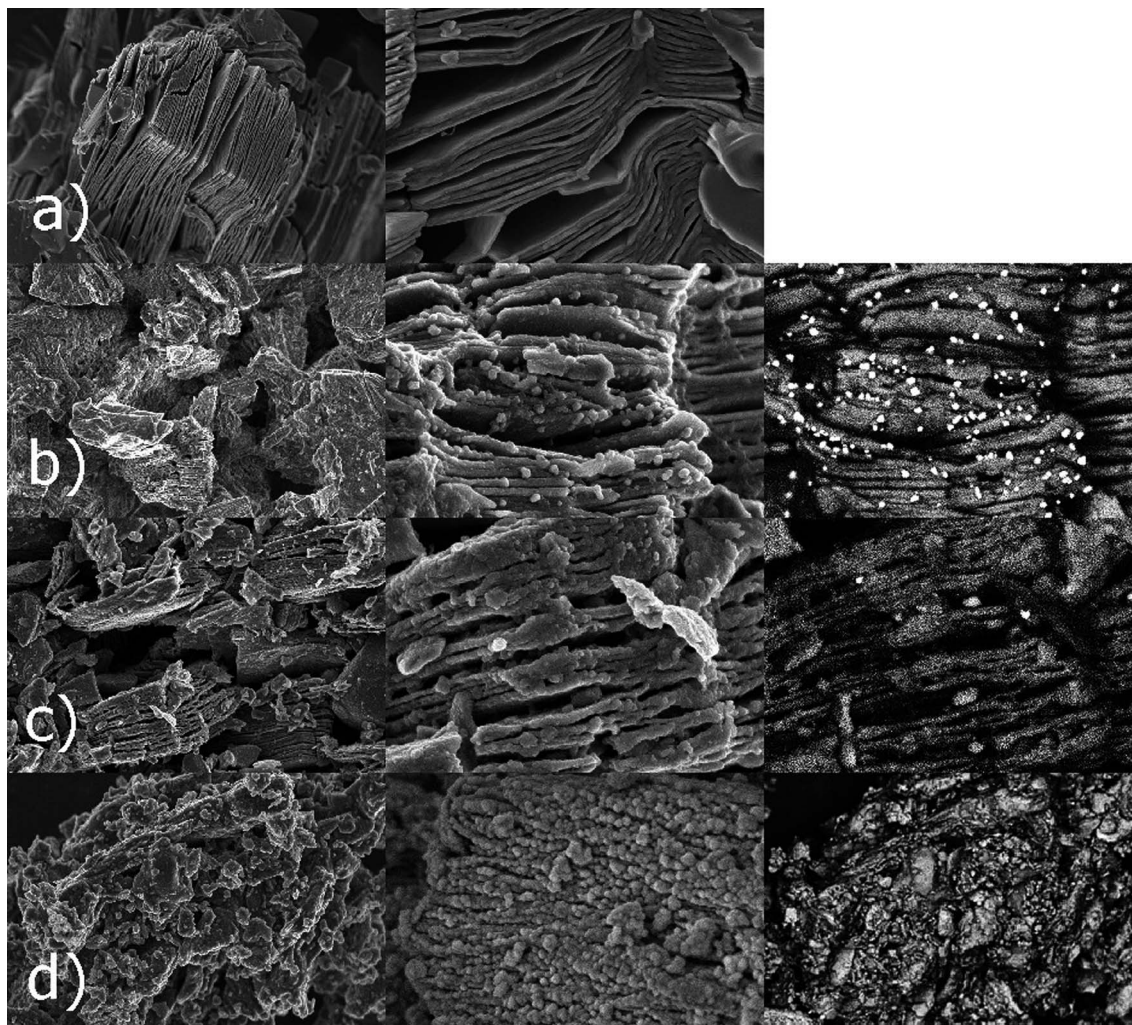
Fig. 1 SEM images obtained for the Ti$_3$C$_2$ MXene (a), Ti$_3$C$_2$/Al$_2$O$_3$/Ag (b), Ti$_3$C$_2$/SiO$_2$/Ag (c), and Ti$_3$C$_2$/SiO$_2$/Pd (d) nanocomposites.

sample, the presence of palladium was confirmed by a Pd-related signal (Fig. 2d).

The quantitative results on the chemical state of the elements present on the surface of the Ti$_3$C$_2$ MXene, as well as nanocomposites of Ti$_3$C$_2$/Al$_2$O$_3$/Ag, Ti$_3$C$_2$/SiO$_2$/Ag, and Ti$_3$C$_2$/SiO$_2$/Pd, are shown in Tables 1–4.

Our results indicated the presence of Ti–C species in the Ti$_3$C$_2$/Al$_2$O$_3$/Ag and Ti$_3$C$_2$/SiO$_2$/Ag nanocomposites by a Ti 2p3 signal located at *ca.* 455 eV which presence is also the characteristic of Ti$_3$C$_2$ MXene (Table 1). The atomic percent of these bonds were, however, different in the investigated nanocomposites, which corresponded with the ceramic oxide/noble metal layer on the surface of Ti$_3$C$_2$ MXene, *i.e.* 1.9 at% in Ti$_3$C$_2$/Al$_2$O$_3$/Ag (Table 2) and 3.4 at% in Ti$_3$C$_2$/SiO$_2$/Ag (Table 3). For Ti$_3$C$_2$/SiO$_2$/Pd (Table 4) the signal coming from Ti–C bonds was not detected due to the large amount of SiO$_2$/Pd nanoparticles covering the Ti$_3$C$_2$ surface with a thick layer (see also Fig. 1d).

XPS investigations also revealed the presence of crystalline TiO$_2$ (by the Ti 2p3 signal located at *ca.* 458 eV) as well as a smaller amount of amorphous phase TiO$_2$ (Ti 2p3 at *ca.* 457 eV). The amount of crystalline TiO$_2$ phase increased between the three investigated nanocomposites, Ti$_3$C$_2$/Al$_2$O$_3$/Ag, Ti$_3$C$_2$/SiO$_2$/Ag, and Ti$_3$C$_2$/SiO$_2$/Pd, *i.e.* 1.5, 3.6, and 6.3 at%, respectively (Tables 2–5). In contrast, the amount of amorphous TiO$_2$ phase was relatively comparable between the Ti$_3$C$_2$/Al$_2$O$_3$/Ag and Ti$_3$C$_2$/SiO$_2$/Ag nanocomposites, *i.e.* 1.1 and 1.8, respectively, and was a little higher for the Ti$_3$C$_2$/SiO$_2$/Pd nanocomposite (3.2 at%).

Our investigations also indicated the presence of different chemical species containing fluorine. For the Ti$_3$C$_2$/Al$_2$O$_3$/Ag nanocomposite, Al–O (F 1s localized at 75.9 eV), Al–F (F 1s localized at 686.9 eV) and C–F (F 1s at 688.4 eV) bonds were detected. For nanocomposites containing silica (*i.e.* Ti$_3$C$_2$/SiO$_2$/Ag and Ti$_3$C$_2$/SiO$_2$/Pd) apart from Si–O connections, the additional Si–F species (Si 2p at 104 eV) were identified (Tables 3 and 4, respectively) and SiO$_2$ (Si 2p signal localized at 103 eV). Also, for the nanocomposites modified with nanosilver, signals corresponding to mainly metallic Ag were detected, *i.e.* Ag 3d5 signal localized at 368.6 eV for Ti$_3$C$_2$/Al$_2$O$_3$/Ag (Table 2) and 367.8 eV for Ti$_3$C$_2$/SiO$_2$/Ag (Table 3). For the Ti$_3$C$_2$/SiO$_2$/Pd nanocomposite (Table 4), the Pd 3d5 signal appeared in the XPS spectrum at 335.2 eV and corresponded to mainly metallic Pd at a level of 0.2 at%. For all the investigated nanocomposites,
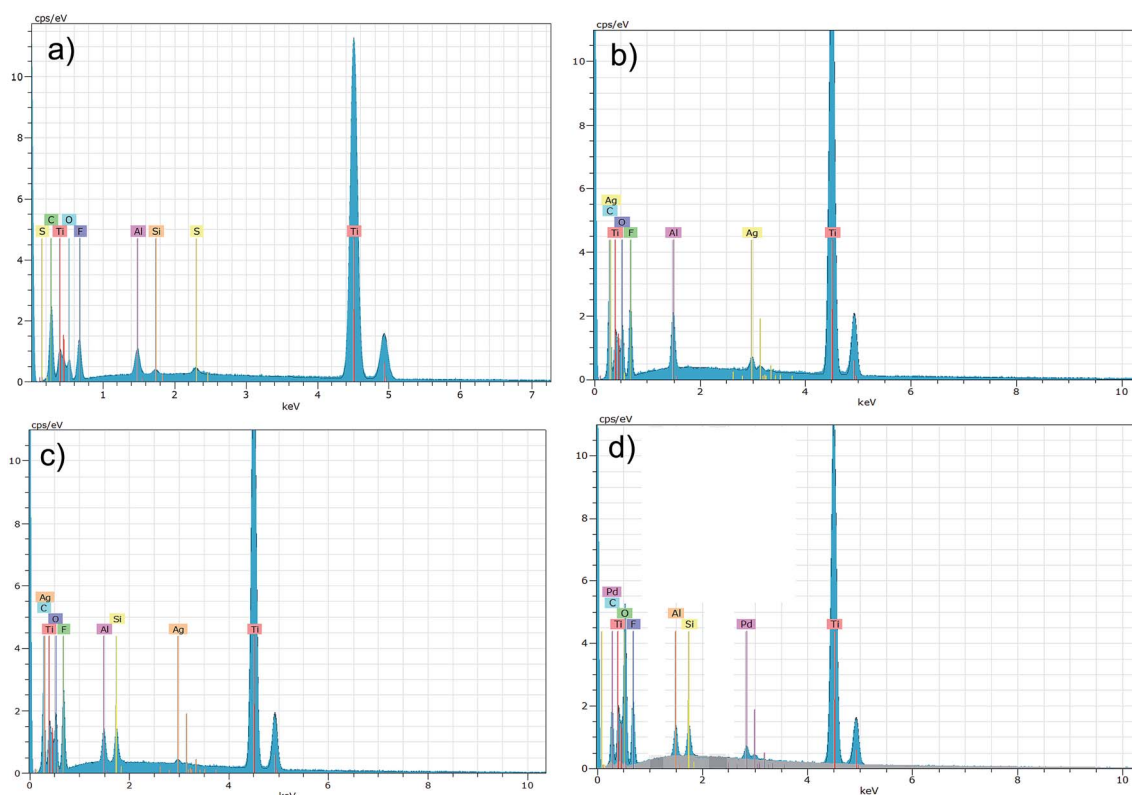
Fig. 2 Results of EDS analysis obtained for the Ti_3C_2 MXene (a) as well as: $Ti_3C_2/Al_2O_3/Ag$ (b), $Ti_3C_2/SiO_2/Ag$ (c), $Ti_3C_2/SiO_2/Pd$ (d) nanocomposites.

some oxidized Ag and Pd were also detected, but in amounts of around 0.1 at%.

We also identified the presence of C=O groups (O 1s signal at *ca.* 533 eV) as well as O=C–OH species (C 1s signal at *ca.* 289 eV) in all the nanocomposites (Tables 2–4). However, they can be related to the surface of Ti_3C_2 as well as to the surfaces of Al_2O_3 or SiO_2 (Table 6).

It should be also noted that the XPS analysis of parent Ti_3C_2 MXene was previously shown in our previous,[7] as well as,[35] the same MXene material was used. In these studies we indicated the presence of surface chemistry typical for MXenes as well as the purity of used material. Our investigations of bioactive

Table 1 Results of XPS analysis combining the chemical state of elements present on the surface of the Ti_3C_2 MXene

Name	Peak BE	At%	SF	Peak BE (−0.9 eV)	Chemical bonds
Ti 2p3	460.3	3.6	5.22	459.4	Ti–O (TiO₂)
Ti 2p3	454.8	2.2	5.22	453.9	Ti–C
Ti 2p3	455.8	5.3	5.22	454.9	Ti–O
Ti 2p3	457.3	4.5	5.22	456.4	Ti–O (amorphous TiO₂)
C 1s	285.0	33.6	1	284.1	C–C
C 1s	281.8	9.0	1	280.9	Ti–C
C 1s	286.6	6.4	1	285.7	C–O
C 1s	288.9	2.4	1	288.0	C=O (O=C–OH)
O 1s	533.8	5.3	2.93	532.9	C–O
O 1s	531.9	6.2	2.93	531.0	Ti–O
O 1s	530.5	4.6	2.93	529.6	C=O
O 1s	535.7	1.1	2.93	534.8	—
F 1s	685.4	9.5	4.43	684.5	Al–F (AlF₃)
F 1s	687.3	2.9	4.43	686.4	Al–F (AlF₃)
F 1s	689.4	0.7	4.43	688.5	C–F
Al 2p	76.3	1.7	0.537	75.4	Al–F (AlF₃)
Al 2p	78.4	0.6	0.537	77.5	Al–F (AlF₃)
Al 2p	73.8	0.7	0.537	72.9	Al–O (Al₂O₃)

Table 2 Results of XPS analysis combining the chemical state of elements present on the surface of the $Ti_3C_2/Al_2O_3/Ag$ nanocomposite

Name	Peak BE	At%	SF	Peak BE (−0.9 eV)	Chemical bonds
Ti 2p3	459.2	1.5	5.22	458.3	Ti–O (TiO₂)
Ti 2p3	455.4	1.9	5.22	454.5	Ti–C
Ti 2p3	457.0	1.1	5.22	456.1	Ti–O (amorphous TiO₂)
C 1s	285.9	29.0	1	285.0	C–C
C 1s	287.5	9.2	1	286.6	C–O
C 1s	290.2	4.4	1	289.3	C=O (O=C–OH)
C 1s	282.0	2.5	1	281.1	Ti–C
O 1s	534.6	9.8	2.93	533.7	C=O
O 1s	531.0	3.9	2.93	530.1	Ti–O
O 1s	533.0	8.0	2.93	532.1	C–O
O 1s	536.0	2.7	2.93	535.1	—
F 1s	687.8	4.2	4.43	686.9	Al–F
F 1s	685.9	2.6	4.43	685.0	Ag–F
F 1s	689.3	1.8	4.43	688.4	C–F
Al 2p	77.2	8.7	0.537	76.3	Al–F
Al 2p	75.9	8.1	0.537	75.0	Al–O
Ag 3d5	368.2	0.3	10.66	367.3	Ag–F
Ag 3d5	369.5	0.2	10.66	368.6	Ag metallic
Ag 3d5	371.1	0.1	10.66	370.2	Ag–O (Ag₂O)

Table 3 Results of XPS analysis combining the chemical state of elements present on the surface of the Ti₃C₂/SiO₂/Ag nanocomposite

Name	Peak BE	At%	SF	Peak BE (−0.54 eV)	Chemical bonds
Ti 2p3	459.7	3.6	5.22	459.1	Ti–O (TiO₂)
Ti 2p3	455.8	3.4	5.22	455.2	Ti–C
Ti 2p3	457.5	1.8	5.22	456.9	Ti–O (amorphous TiO₂)
Ti 2p3	461.5	0.7	5.22	461.0	Ti–O (TiO₂)
C 1s	285.5	26.5	1	285.0	C–C
C 1s	282.2	4.2	1	281.6	Ti–C
C 1s	287.0	9.9	1	286.4	C–O
C 1s	289.5	4.4	1	288.9	C=O (O=C–OH)
O 1s	533.7	17.4	2.93	533.1	C–O
O 1s	531.3	8.5	2.93	530.7	Ti–O
O 1s	535.3	9.6	2.93	534.8	C=O
F 1s	687.2	1.0	4.43	686.7	Si–F
F 1s	689.2	0.9	4.43	688.7	C–F
F 1s	691.1	0.3	4.43	690.5	Ag–F
F 1s	685.4	1.2	4.43	684.9	Al–F
Si 2p	105.3	3.3	0.817	104.8	Si–F
Si 2p	107.2	0.9	0.817	106.6	—
Si 2p	103.8	2.4	0.817	103.2	Si–O (SiO₂)
Ag 3d5	368.3	0.0	10.66	367.8	Ag metallic
Ag 3d3	374.3	0.0	7.38	373.8	Ag–O (Ag₂O)

properties toward model Gram-negative *Escherichia coli* bacterial strain also showed that antibacterial properties of the Ti₃C₂ MXene.[7]

An analysis of physical properties and porous structures of Ti₃C₂ MXene and the Ti₃C₂/Al₂O₃/Ag, Ti₃C₂/SiO₂/Ag, and Ti₃C₂/SiO₂/Pd nanocomposites was carried out, based on the isotherms of physical nitrogen sorption. The obtained isotherms are shown in Fig. 3. The obtained results indicated that the Ti₃C₂/SiO₂/Pd nanocomposite adsorbed almost twice as much nitrogen as the other modified samples. As can be seen in Fig. 1d, the Ti₃C₂ MXene is covered with SiO₂/Pd nanoparticles which are much more dispersed in comparison to SiO₂/Ag

(Fig. 1c). This effect has been also observed for TiO₂/Pd nanocomposite structures.[36] Palladium usually promotes better dispersion. This effect typically results in higher surface are but is not strictly connected with toxicity because nanoparticles are attached to the surface of Ti₃C₂ MXene.

The shape of the obtained isotherms suggested the presence of not only slit pores, which are also characteristic for graphenes, but also cylindrical ones.[37,38]

The results of the physical properties of the analyzed samples are presented in Table 5. As expected, the BET specific surface area of the pure Ti₃C₂ was significantly larger than the specific surface area of modified samples. The total volume of

Table 4 Results of XPS analysis combining the chemical state of elements present on the surface of the Ti₃C₂/SiO₂/Pd nanocomposite

Name	Peak BE	At%	SF	Peak BE (−0.56 eV)	Chemical bonds
Ti 2p3	459.7	6.3	5.22	459.1	Ti–O (TiO₂)
Ti 2p3	461.1	3.2	5.22	460.5	Ti–O (amorphous TiO₂)
C 1s	285.6	30.9	1	285.0	C–C
C 1s	287.1	12.8	1	286.5	C–O
C 1s	289.3	5.2	1	288.7	C=O (O=C–OH)
C 1s	290.3	1.7	1	289.8	C–O/C–F
O 1s	531.1	13.7	2.93	530.5	Ti–O
O 1s	532.8	11.4	2.93	532.2	C–O
O 1s	534.3	7.5	2.93	533.8	C=O
O 1s	535.9	2.3	2.93	535.3	—
F 1s	685.3	1.2	4.43	684.8	Al–F
F 1s	687.2	0.8	4.43	686.7	Si–F
F 1s	689.2	0.5	4.43	688.7	C–F
F 1s	691.4	0.2	4.43	690.8	Pd–F
Si 2p	104.9	1.0	0.817	104.3	Si–F
Si 2p	103.3	0.6	0.817	102.8	Si–O (SiO₂)
Si 2p	106.6	0.4	0.817	106.1	—
Pd 3d5	335.7	0.2	9.48	335.2	Pd metallic
Pd 3d5	337.4	0.1	9.48	336.9	Pd–O (PdO)
Pd 3d5	338.8	0.1	9.48	338.3	Pd–O (PdO₂)

Table 5 The results of the physical properties of the Ti$_3$C$_2$ MXene and Ti$_3$C$_2$/Al$_2$O$_3$/Ag, Ti$_3$C$_2$/SiO$_2$/Ag, and Ti$_3$C$_2$/SiO$_2$/Pd nanocomposites

	S_{BET}	V_{BJH}	r_{BJH}	$S_{t\text{-ext}}$	$S_{t\text{-micr}}$	$V_{t\text{-micr}}$
Ti$_3$C$_2$ MXene (reference sample)	80.08	0.0868	15.33	54.40	25.68	0.0152
Ti$_3$C$_2$/3% Al$_2$O$_3$/2% Ag	14.81	0.02408	14.92	11.95	2.859	0.0007748
Ti$_3$C$_2$/3% SiO$_2$/2% Ag	14.92	0.05043	19.83	14.92	—	—
Ti$_3$C$_2$/3% SiO$_2$/2% Pd	56.71	0.05050	25.90	31.67	25.04	0.01596

Table 6 Summary of the antibacterial properties of the Ti$_3$C$_2$ MXene, Ti$_3$C$_2$/Al$_2$O$_3$/Ag, Ti$_3$C$_2$/SiO$_2$/Ag, and Ti$_3$C$_2$/SiO$_2$/Pd nanocomposite

| Sample name	Influence on the particular bacteria species
Ti$_3$C$_2$ MXene (reference sample)	*Escherichia coli* − *Sarcina lutea* − *Staphylococcus aureus* + *Bacillus* sp. −
Ti$_3$C$_2$/3% Al$_2$O$_3$/2% Ag	*Escherichia coli* + *Sarcina lutea* ++ *Staphylococcus aureus* + *Bacillus* sp. +
Ti$_3$C$_2$/3% SiO$_2$/2% Ag	*Escherichia coli* ++ *Sarcina lutea* ++ *Staphylococcus aureus* + *Bacillus* sp. +
Ti$_3$C$_2$/3% SiO$_2$/2% Pd	*Escherichia coli* ++ *Sarcina lutea* ++ *Staphylococcus aureus* + *Bacillus* sp. +

pores (V_{BJH}) was larger in the unmodified Ti$_3$C$_2$ than in the modified samples. It was due to the nanoparticles which filled the open slit-shaped pores of the parent MXene. The same effect was previously seen for covalent modifications of graphene oxide with nanoparticles.[37,38]

The pore size distributions obtained for Ti$_3$C$_2$ MXene, Ti$_3$C$_2$/Al$_2$O$_3$/Ag, Ti$_3$C$_2$/SiO$_2$/Ag, and Ti$_3$C$_2$/SiO$_2$/Pd are presented in Fig. 4. The obtained BJH results indicate that, in all of our materials, there were mainly micropores (in the range of 3–6 nm) present. As can be also observed, mesopores (in the range of 5–50 nm) were present in small quantities in comparison to the general amount of micropores.

The investigations of the bioactive properties of the samples, performed using the classical culture method, revealed that the modification of Ti$_3$C$_2$ MXene with Al$_2$O$_3$ + Ag, SiO$_2$ + Ag, and SiO$_2$ + Pd resulted in significantly increased antibacterial properties (Fig. 5); the results of the experiment with *Staphylococcus aureus*, with an application of the dilution method revealed that all the tested samples were able to inhibit the growth of potentially pathogenic bacterial strains (Fig. 6). The considered mechanism of action for Ti$_3$C$_2$ MXene is related to the direct physical interactions between the edges of the nanosheets and the surface of bacterial cell wall or membrane. The Ti$_3$C$_2$ MXene nanosheets were previously found to damage physically the microorganisms' cells.[39] As a result cells lose their integrity and the internal cytoplasm was released together with DNA.

Some differences in the optical density of the bacterial culture (reflecting the differences in the number of bacterial cells) were observed in low concentrations of nanocomposites. Ti$_3$C$_2$ MXene appeared as the most biocidal particle. However, in higher nanoparticles concentrations the antimicrobial properties of tested nanocompounds were similar despite Ti$_3$C$_2$/SiO$_2$/Ag in concentration 500 mg l^{-1}. It can be stated that the modification of Ti$_3$C$_2$ MXene probably does not influence significantly its antimicrobial properties. When taking into consideration systems where ceramic nanoparticles are present or noble metal nanoparticles, different effects should be considered. It should be noted, that when nanoparticles are
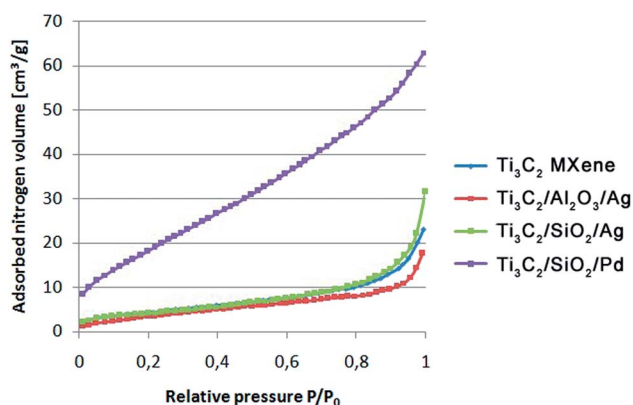
Fig. 3 Nitrogen sorption isotherms obtained for the Ti$_3$C$_2$ MXene, Ti$_3$C$_2$/Al$_2$O$_3$/Ag, Ti$_3$C$_2$/SiO$_2$/Ag, and Ti$_3$C$_2$/SiO$_2$/Pd nanocomposites.
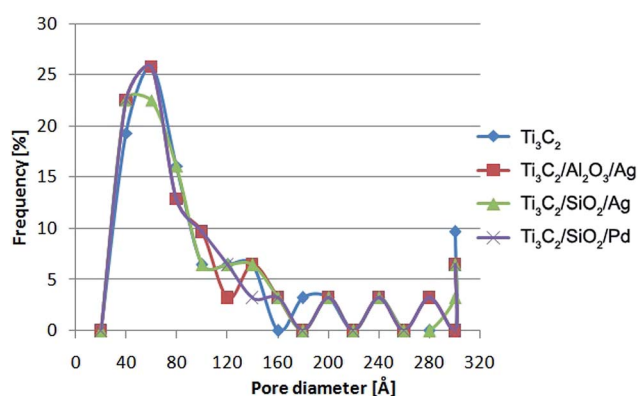
Fig. 4 The distributions of pore diameter obtained using BJH method for the Ti$_3$C$_2$ MXene, Ti$_3$C$_2$/Al$_2$O$_3$/Ag, Ti$_3$C$_2$/SiO$_2$/Ag, and Ti$_3$C$_2$/SiO$_2$/Pd nanocomposites.
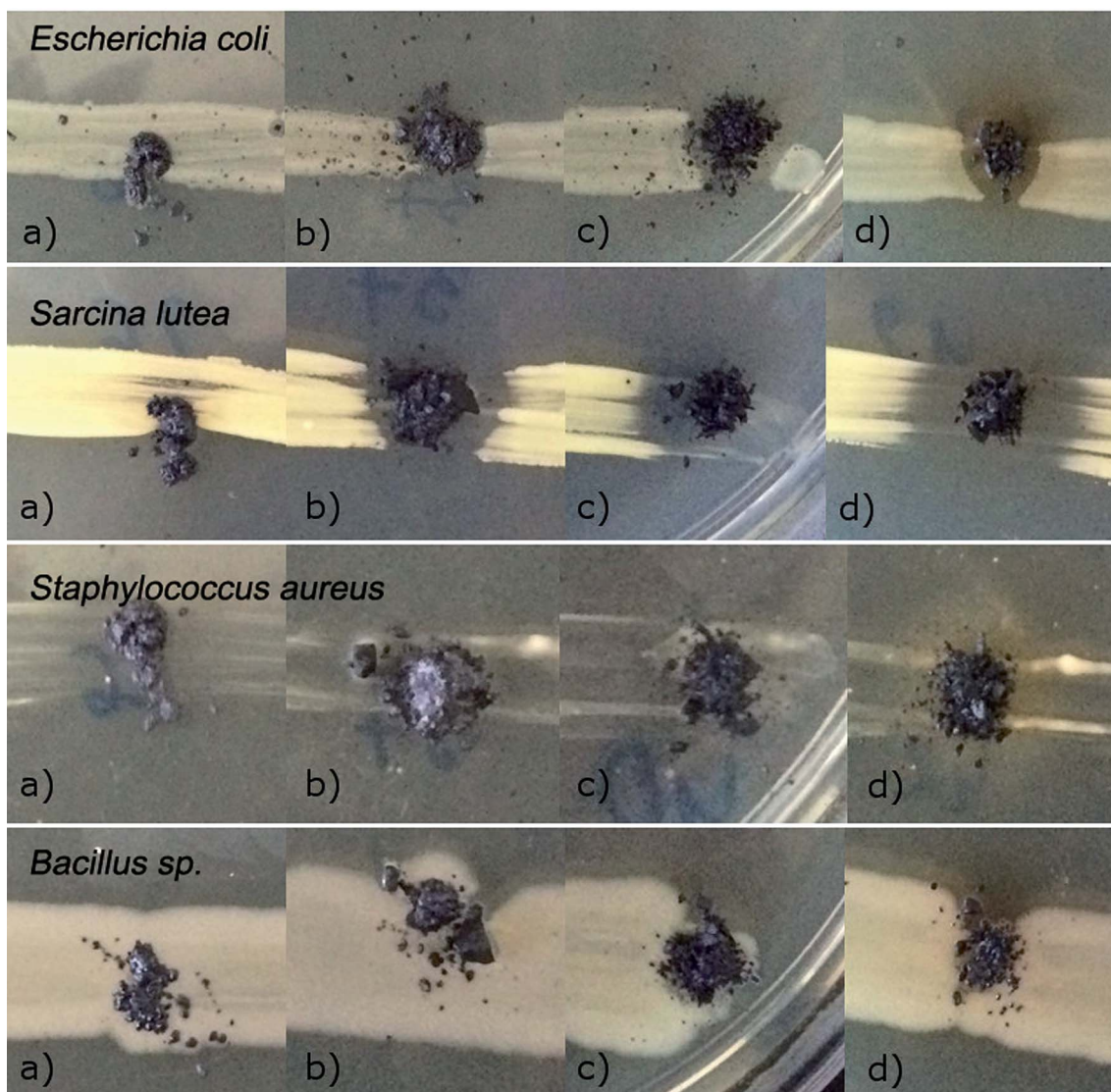
Fig. 5 Growth of *Escherichia coli*, *Sarcina lutea*, *Staphylococcus aureus*, and *Bacillus* sp. bacteria strains in the presence of Ti_3C_2 MXene (a), $Ti_3C_2/Al_2O_3/Ag$ (b), $Ti_3C_2/SiO_2/Ag$ (c), and $Ti_3C_2/SiO_2/Pd$ (d) nanocomposite structures.
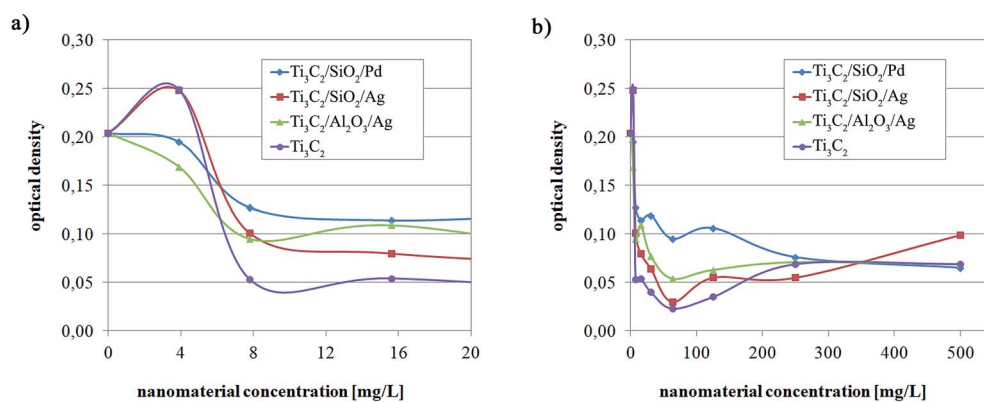
Fig. 6 Antibacterial impact of Ti_3C_2 MXene, $Ti_3C_2/Al_2O_3/Ag$, $Ti_3C_2/SiO_2/Ag$, and $Ti_3C_2/SiO_2/Pd$ nanocomposite against *Staphylococcus aureus* bacteria. The results are presented in the range of 0–20 mg l^{-1} (a), and 0-500 mg l^{-1} (b) of nanomaterial concentration.

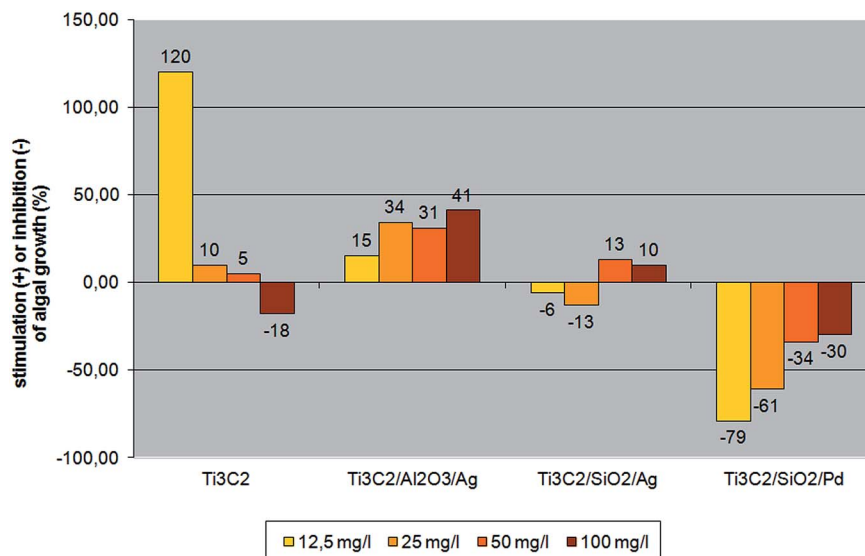**Fig. 7** Stimulation/inhibition of algal growth in the presence of pristine Ti_3C_2 MXene, $Ti_3C_2/Al_2O_3/Ag$, $Ti_3C_2/SiO_2/Ag$, and $Ti_3C_2/SiO_2/Pd$ nanocomposite, at different concentrations, after 14 days of incubation.

present on the surface of Ti_3C_2, the sharp edges are also covered with nanoparticles (Fig. 1). Moreover, nanoparticles are strongly attached to the surface of Ti_3C_2 such as it was previously considered for modifications of graphene oxide.[33,40] Accordingly, the antimicrobial effect relates to the presence of bioactive noble metal nanoparticles.[41] Because they are incorporated into ceramic Al_2O_3 or SiO_2 (*i.e.* immobilized in a porous Al_2O_3 or SiO_2 matrix) – the only bioactive agent can be Ag^+ or Pd^+ ions. These ions are mostly active when direct contact occur or when the basic material (*i.e.* MXene). Additionally, the possibility of promoting of bioactive ions release should be considered for Ti_3C_2. It was previously shown, that the presence of graphene oxide in a core of a core–shell hybrid changes bioactivity of a system due to changes of zeta potential which can influence releasing of active ions.[42]

Nowadays, numerous nanoproducts are introduced into aquatic environments with wastewater streams.[43] The estimation of nanomaterial toxicity to algae is essential because algae serve as the basis of numerous aquatic food chains. Some toxicity tests of nanoparticles' influence on the microalgae *Pseudokirchneriella subcapitata* have been carried out.[44] The impact of ZnO, TiO_2, and CuO nanoparticles on the prolongation of the lag phase of growth of *Pseudokirchneriella subcapitata* was observed. The formation of characteristic aggregates entrapping algal cells was revealed for nano-TiO_2.[45] The experiment carried out by Karwowska *et al.*[46] on Al_2O_3 nanopowders' influence on green algae *Scenedesmus quadricauda* revealed that after 7 days the algal growth was inhibited by 5–54% in nanopowder concentrations of 500 mg l^{-1}, while in concentrations of 1000 mg l^{-1} it reached 39–69%, depending on the properties of the individual nanopowder. Marine phytoplankton, including *Thalassiosira pseudonana*, *Skeletonema marinoi*, *Dunaliella tertiolecta*, and *Isochrysis galbana*, were also affected by metal oxide nanoparticles.[47] It has been confirmed that a nanoproduct's

toxicity depends on its concentration, physico-chemical properties, and the environmental conditions.[48]

The results obtained in the present experiment showed that the impact of individual nanocomposites on tested algae differed, depending both on the concentration and the type of nanocomponents (Fig. 7). Pristine Ti_3C_2 MXene at the lowest concentration significantly stimulated algal growth. With increasing nanocomponent concentration, the stimulation effect diminished: for a concentration of 100 mg l^{-1}, an inhibition of the bacterial effect was observed. The effect of growth intensification is also known for *Monoraphidium minutum* in presence of cobalt.[49] Also arsenic was reported to stimulate the growth of microalgae *Chlorella* sp.[50,51] This effect is related to the effect of dissolution of inorganic ions which support microalgae growth. The six times growth intensification of *Scenedesmus* was observed when vanadium was present. The vanadium ions were therefore almost entirely consumed by algae cells.[52]

It should be mentioned that algae are very sensitive for even small changes in chemical composition of the tested material as well as its concentration.[53] Indeed, four different analysed compositions (*i.e.* $Ti_3C_2/Al_2O_3/Ag$, $Ti_3C_2/SiO_2/Ag$ and $Ti_3C_2/SiO_2/Pd$) showed different effects on algae and those effects became more viable when concentration was changed. There were considered two variants of material composition *i.e.*: (i) the same basic composition (Ti_3C_2 and Ag) and changing the type of ceramic used *i.e.* Al_2O_3 or SiO_2, and (ii) the same basic composition (Ti_3C_2 and SiO_2) and changing the type of noble metal used *i.e.* Ag or Pd. For both cases, different bio-effects were observed for green algae *i.e.* (1) the presence of Al_2O_3 at the material surface results in lower toxicity than presence of SiO_2; (2) presence of Pd at the material surface results in much higher toxicity than presence of Ag. Different metallic and ceramic oxide nanoparticles were reported to exhibit the
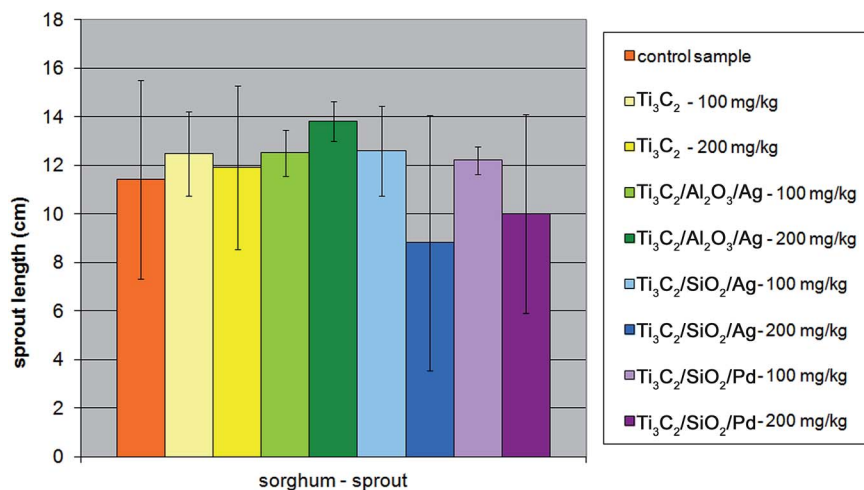
Fig. 8 The influence of tested nanopowders at concentrations of 100 mg kg^{-1} and 200 mg kg^{-1} on the growth of the sprout of *Sorghum saccharatum*.

inhibitory activity of algae growth due to Reactive Oxygen Species (ROS) generation,[54,55] the physical interactions,[56] releasing of metal ions from the surface of the nano-material[55,57] as well as their sizes.[54] The probable mechanism of action that should be considered for the analyses nano-composite materials is the presence of different ceramic oxide and noble metal components is the surface-dissolution of as well as physical interaction with algae cells.[46,53,58] Ti$_3$C$_2$/Al$_2$O$_3$/Ag nanoparticles stimulated algal growth, with an increasing effect being caused by higher nanoparticle concentrations. The results obtained for Ti$_3$C$_2$/SiO$_2$/Ag indicated both slight inhibition/stimulation. Ti$_3$C$_2$/SiO$_2$/Pd nanocomposite revealed the strongest ecotoxic impact on *Desmodesmus quadricauda*, with the inhibition effectiveness increasing with a decreasing concentration of the nanopowder. It could be caused by an aggregating effect in the algal culture medium for the higher nanocomposite concentrations. It is evident that further study, covering the analysis of the mechanism of interaction between pristine Ti$_3$C$_2$ MXene and its derivatives, is necessary to explain this phenomenon.

The experiments performed in the present study, carried out in the presence of two comparatively high concentrations of nanocomposites – 100 mg l^{-1} and 200 mg l^{-1}, revealed that SiO$_2$-containing nanocomponents could influence the growth of the sprout and root of *Sorghum saccharatum* compared with the control sample. The inhibition effect was even stronger at a concentration of 200 mg kg^{-1} of the soil. The effect was not observed for the Al$_2$O$_3$-modified nanocomposite and the pristine Ti$_3$C$_2$ MXene (Fig. 8 and 9).

In the case of charlock (*Sinapis alba*), all the modifications of the Ti$_3$C$_2$ MXene nanocomposite resulted in a decrease in phytotoxic properties towards the plant's sprout, although the root growth of the plant was not inhibited only in the presence of the Ti$_3$C$_2$/Al$_2$O$_3$/Ag nanocompound (Fig. 10 and 11). The strongest inhibition of the seed germination (up to 40%) was observed for the Ti$_3$C$_2$ MXene, while it did not exceed 20% in the presence of the other tested nanocomposites.

There is evidence that several inorganic nano-oxides may interact with plant cells. The mechanisms for plant root adsorption and incorporation into the cell wall or cell membrane have already been studied, although there is still a lack of knowledge concerning the nanoparticles' internalization.[59] It has been confirmed that nanoparticles can influence both the cell structures and physiological mechanisms, bonding to different intracellular structures, including the Golgi apparatus and endoplasmic reticulum. One of the recognized mechanisms is the ability to form reactive oxygen species.[60] Accordingly, we can now understand better the reactivity of surface-modified MXenes towards chosen organisms, giving more information concerning the potential impact of tested nanocomposite structures on the ecosystems. The further investigations between Ti$_3$C$_2$ MXenes and plant cells will be undoubtedly a subject of future research for scientific community working with MXenes.

4. Summary

The number of investigations regarding the application of 2D nanosheets of MXenes in different technological areas is growing rapidly. Different surface modifications of MXenes have been introduced to date in order to tailor their properties. As a result, surface-modified MXenes could be released in the environment from filtration membranes, adsorbents, or photocatalysts. On the other hand, assessment of their environmental impact is practically unexplored. So far, the only publication in this area is Nasrallah *et al.*,[1] who reported the lack of significant toxicity of pristine Ti$_3$C$_2$ MXene towards zebrafish embryos. In the present study, we made some preliminary tests allowing to evaluate how modification of the antimicrobial Ti$_3$C$_2$ MXene with ceramic oxide and noble metal nanoparticles can influence its toxicity. The ecotoxicological assessment covered the experiments with a application of the green algae *Desmodesmus quadricauda* as well as higher plants – sorghum (*Sorghum saccharatum*) and charlock (*Sinapis alba*).
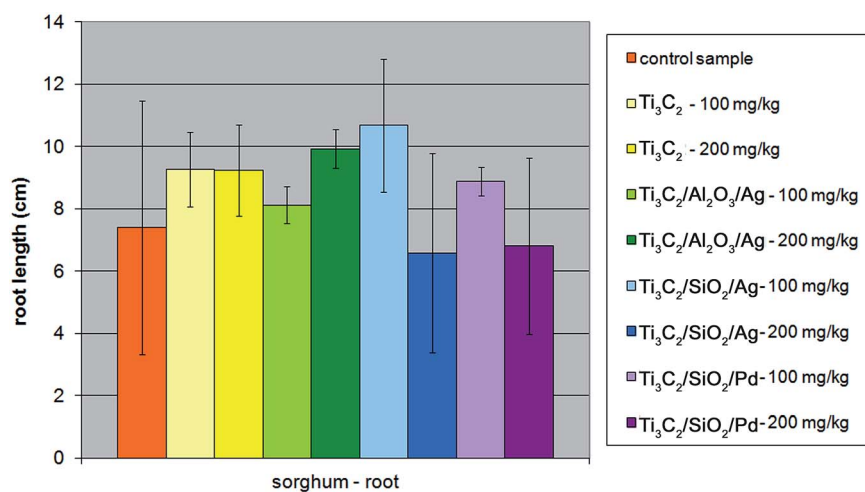
Fig. 9 The influence of tested nanopowders at concentrations of 100 mg kg^{-1} and 200 mg kg^{-1} on the growth of the root of *Sorghum saccharatum*.
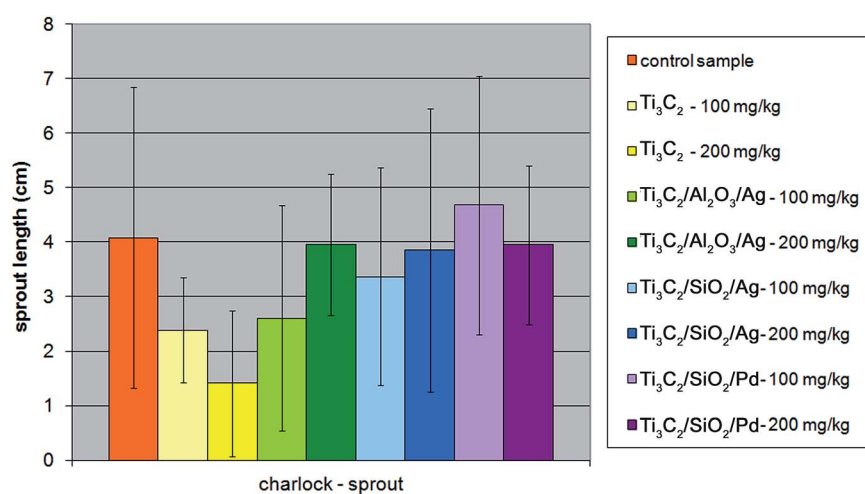

Fig. 10 The influence of tested nanopowders at concentrations of 100 mg kg^{-1} and 200 mg kg^{-1} on the growth of the sprout of *Sinapis alba*.

It was observed that in the growth tests on solid media all the modifications of the pristine Ti_3C_2 MXene influenced positively its antibacterial properties against both Gram-positive and Gram-negative bacteria, despite a *Staphylococcus aureus* strain, in which effect was similar for all the nanocompounds. The last effect was also confirmed using the dilution method.

Our examinations of the ecotoxicity and phytotoxicity of the tested nanocomposites have shown that their ecotoxicity against algae depended not only on their concentration, but also on the type of modification. Both stimulating and inhibiting effects were observed for individual nanocomposites. We have observed that pristine Ti_3C_2 which highly stimulated green algae growth at low concentrations. The strongest anti-algal effect, especially in case of low concentrations, was observed for $Ti_3C_2/SiO_2/Pd$ nanocomposite.

The modifications of the pristine Ti_3C_2 MXene influenced its phytotoxic properties. The addition of SiO_2/Ag or SiO_2/Pd made it more phytotoxic, although the effect was not noted for

$Ti_3C_2/Al_2O_3/Ag$. Germination inhibition was lower in modified nanocomposites compared with the pristine Ti_3C_2 MXene.

It is evident that the modification of the pristine Ti_3C_2 MXene with different nanoparticles can change its ecotoxicity. Some of modified nanocompounds can be more eco- or phytotoxic to organisms playing the essential role of the primary producers in natural ecosystems. However, we have indicated nanocomposite structures characterized by significantly decreased ecotoxic properties: Ti_3C_2 MXene modified with Al_2O_3/Ag. The increase of antibacterial activity resulting from the modification of the pristine Ti_3C_2 MXene make them useful as the biocidal agents. On the other hand, the application of MXenes in different technologies should give rise to special attention to their toxicity, due to their potential ecotoxic properties. The results of our work confirm that modification of MXenes can result in the change of its potential toxic properties. Ti_3C_2 MXene modified with Al_2O_3/Ag was neither phyto- nor ecotoxic but still characterized by antimicrobial properties, which
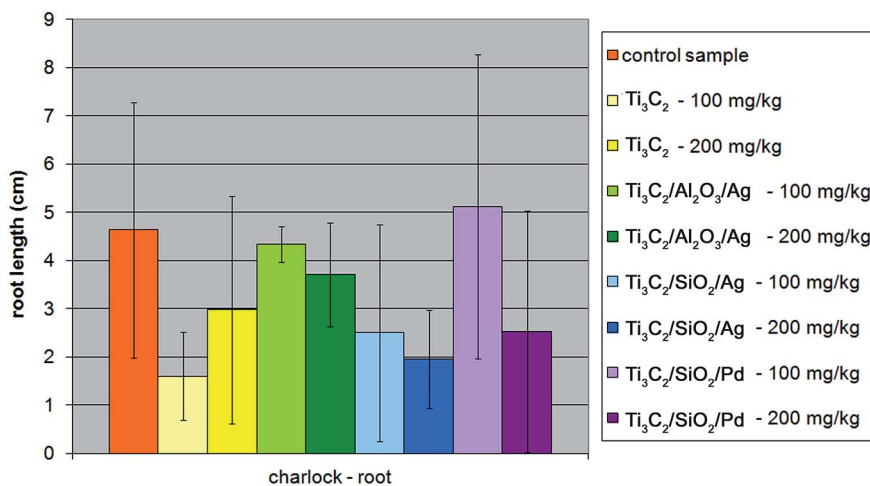
Fig. 11 The influence of tested nanopowders at concentrations of 100 mg kg^{-1} and 200 mg kg^{-1} on the growth of the root of *Sinapis alba*.

can be important from the point of view of its potential application in practice.

Authors' contributions

A. Rozmysłowska-Wojciechowska collected the obtained results, prepared the final version of the manuscript; carried out analysis of morphology, structure, physical properties and porous structure of the obtained materials; S. Poźniak was involved in the analysis of physical properties and porous structure of the obtained materials as well as preparation of figures, tables and interpretation of the results; E. Karwowska carried out and interpreted microbiological and ecotoxicity tests; T. Wojciechowski synthesized the expanded Ti$_3$C$_2$ MXene material and modified it with ceramic and noble metal nanoparticles; L. Chlubny synthesized the MAX phase using SHS method; A. Olszyna revised the characterization part of the manuscript. W. Ziemkowska supervised MXene preparation and modification; A. M. Jastrzębska supervised the whole research and coordinated the preparation of the manuscript. All the authors read and approved the manuscript.

Conflicts of interest

The authors declare that there is no conflict of interest regarding publication of this manuscript.

Acknowledgements

Notes and references

1 G. K. Nasrallah, M. Al-Asmakh, K. Rasool and K. A. Mahmoud, Ecotoxicological assessment of Ti$_3$C$_2$T$_x$ (MXene) using a zebrafish embryo model, *Environ. Sci.: Nano*, 2018, **5**, 1002–1011.

2 M. Naguib, O. Mashtalir, J. Carle, V. Presser, J. Lu, L. Hultman, Y. Gogotsi and M. W. Barsoum, Two-dimensional transition metal carbides, *ACS Nano*, 2012, **6**, 1322–1331.

3 A. Shahzad, K. Rasool, W. Miran, M. Nawaz, J. Jang, K. A. Mahmoud and D. S. Lee, Two-Dimensional Ti$_3$C$_2$T$_x$ MXene Nanosheets for Efficient Copper Removal from Water, *ACS Sustainable Chem. Eng.*, 2017, **5**, 11481–11488.

4 O. Mashtalir, K. M. Cook, V. N. Mochalin, M. Crowe, M. W. Barsoum and Y. Gogotsi, Dye adsorption and decomposition on two-dimensional titanium carbide in aqueous media, *J. Mater. Chem. A*, 2014, **2**, 14334–14338.

5 K. Rasool, M. Helal, A. Ali, C. E. Ren, Y. Gogotsi and K. A. Mahmoud, Antibacterial Activity of Ti$_3$C$_2$T$_x$ MXene, *ACS Nano*, 2016, **10**, 3674–3684.

6 A. A. Shamsabadi, M. Sharifian Gh., B. Anasori and M. Soroush, Antimicrobial Mode-of-Action of Colloidal Ti$_3$C$_2$T$_x$ MXene, *ACS Sustainable Chem. Eng.*, 2018, **6**, 16586–16596.

7 A. M. Jastrzębska, E. Karwowska, T. Wojciechowski, W. Ziemkowska, A. Rozmysłowska, L. Chlubny and A. Olszyna, The Atomic Structure of Ti$_2$C and Ti$_3$C$_2$ MXenes is Responsible for Their Antibacterial Activity Toward *E. coli* Bacteria, *J. Mater. Eng. Perform.*, 2018, 1–6, DOI: 10.1007/s11665-018-3223-z.

8 A. Jastrzębska, E. Karwowska, D. Basiak, A. Zawada, W. Ziemkowska, T. Wojciechowski, D. Jakubowska and A. Olszyna, Biological Activity and Bio-Sorption Properties of the Ti$_2$C Studied by Means of Zeta Potential and SEM, *Int. J. Electrochem. Sci.*, 2017, **12**, 2159–2172.

9 Z. Wei, Z. Peigen, T. Wubian, W. Ying, Z. Yamei, C. Jian and S. ZhengMing, Microwave-assisted synthesis of SnO$_2$-Ti$_3$C$_2$ nanocomposite for enhanced supercapacitive performance, *Mater. Lett.*, 2017, **209**, 122–125.

10 F. Wang, Z. Wang, J. Zhu, H. Yang, X. Chen, L. Wang and C. Yang, Facile synthesis SnO$_2$ nanoparticle-modified Ti$_3$C$_2$ MXene nanocomposites for enhanced lithium storage application, *J. Mater. Sci.*, 2017, **52**, 3556–3565.

11 C. Peng, H. Wang, H. Yu and F. Peng, TiO_{2-x}/Ti_3C_2: synergy of active facets, interfacial charge transfer and Ti^{3+} doping for enhance photocatalytic activity, *Mater. Res. Bull.*, 2017, **89**, 16–25.

12 M. Xue, Z. Wang, F. Yuan, X. Zhang, W. Wei, H. Tang and C. Li, Preparation of $TiO_2/Ti_3C_2T_x$ hybrid nanocomposites and their tribological properties as base oil lubricant additives, *RSC Adv.*, 2017, **7**, 4312–4319.

13 C. J. Zhang, S. J. Kim, M. Ghidiu, M. Zhao, M. W. Barsoum, V. Nicolosi and Y. Gogotsi, Layered Orthorhombic $Nb_2O_5@Nb_4C_3T_x$ and $TiO_2@Ti_3C_2T_x$ Hierarchical Composites for High Performance Li-ion Batteries, *Adv. Funct. Mater.*, 2016, **26**, 4143–4151.

14 H. Tang, S. Zhuang, Z. Bao, C. Lao and Y. Mei, Two-Step Oxidation of Mxene in the Synthesis of Layer-Stacked Anatase Titania with Enhanced Lithium-Storage Performance, *ChemElectroChem*, 2016, **3**, 871–876.

15 C. Peng, X. Yang, Y. Li, H. Yu, H. Wang and F. Peng, Hybrids of Two-Dimensional Ti_3C_2 and TiO_2 Exposing {001} Facets toward Enhanced Photocatalytic Activity, *ACS Appl. Mater. Interfaces*, 2016, **8**, 6051–6060.

16 F. Wang, C. Yang, M. Duan, Y. Tang and J. Zhu, TiO_2 nanoparticle modified organ-like Ti_3C_2 MXene nanocomposite encapsulating hemoglobin for a mediator-free biosensor with excellent performances, *Biosens. Bioelectron.*, 2015, **74**, 1022–1028.

17 Y. Gao, L. Wang, A. Zhou, Z. Li, J. Chen, H. Bala, Q. Hu and X. Cao, Hydrothermal synthesis of A. TiO_2/Ti_3C_2 nanocomposites with enhanced photocatalytic activity, *Mater. Lett.*, 2015, **150**, 62–64.

18 H. Ghassemi, W. Harlow, O. Mashtalir, M. Beidaghi, M. R. Lukatskaya, Y. Gogotsi and M. L. Taheri, *In situ* environmental transmission electron microscopy study of oxidation of two-dimensional Ti_3C_2 and formation of carbon-supported TiO_2, *J. Mater. Chem. A*, 2014, **2**, 14339–14343.

19 H. Zhang, H. Dong, X. Zhang, Y. Xu and J. Fransaer, Cu_2O Hybridized Titanium Carbide with Open Conductive Frameworks for Lithium-ion Batteries, *Electrochim. Acta*, 2016, **202**, 24–31.

20 Y. Gao, L. Wang, Z. Li, A. Zhou, Q. Hu and X. Cao, Preparation of MXene-Cu_2O nanocomposite and effect on thermal decomposition of ammonium perchlorate, *Solid State Sci.*, 2014, **35**, 62–65.

21 M. Ming, Y. Ren, M. Hu, Y. Zhang, T. Sun, Y. Ma, X. Li, W. Jiang, D. Gao, J. Bi and G. Fan, Promoted effect of alkalization on the catalytic performance of Rh/alk-$Ti_3C_2X_2$ (XO, F) for the hydrodechlorination of chlorophenols in base-free aqueous medium, *Appl. Catal., B*, 2017, **210**, 462–469.

22 X. Li, G. Fan and C. Zeng, Synthesis of ruthenium nanoparticles deposited on graphene-like transition metal carbide as an effective catalyst for the hydrolysis of sodium borohydride, *Int. J. Hydrogen Energy*, 2014, **39**, 14927–14934.

23 X. Li, C. Zeng and G. Fan, Ultrafast hydrogen generation from the hydrolysis of ammonia borane catalyzed by highly efficient bimetallic RuNi nanoparticles stabilized on

$Ti_3C_2X_2$ (X = OH and/or F), *Int. J. Hydrogen Energy*, 2014, **40**, 3883–3891.

24 Z. Guo, T. Liu, Q. Wang and G. Gao, Construction of cost-effective bimetallic nanoparticles on titanium carbides as a superb catalyst for promoting hydrolysis of ammonia borane, *RSC Adv.*, 2018, **8**, 843–847.

25 Q. Xue, Z. Pei, Y. Huang, M. Zhu, Z. Tang, H. Li, Y. Huang, N. Li, H. Zhang and C. Zhi, Mn_3O_4 nanoparticles on layer-structured Ti_3C_2 MXene towards the oxygen reduction reaction and zinc–air batteries, *J. Mater. Chem. A*, 2017, **5**, 20818–20823.

26 R. B. Rakhi, B. Ahmed, D. Anjum and H. N. Alshareef, Direct Chemical Synthesis of MnO_2 Nanowhiskers on Transition-Metal Carbide Surfaces for Supercapacitor Applications, *ACS Appl. Mater. Interfaces*, 2016, **8**, 18806–18814.

27 X. Guo, X. Xie, S. Choi, Y. Zhao, H. Liu, C. Wang, S. Chang and G. Wang, Sb_2O_3/MXene($Ti_3C_2T_x$) hybrid anode materials with enhanced performance for sodium-ion batteries, *J. Mater. Chem. A*, 2017, **5**, 12445–12452.

28 Q. X. Xia, J. Fu, J. M. Yun, R. S. Mane and K. H. Kim, High volumetric energy density annealed-MXene-nickel oxide/MXene asymmetric supercapacitor, *RSC Adv.*, 2017, **7**, 11000–11011.

29 C. Ling, L. Shi, Y. Ouyang, Q. Chen and J. Wang, Transition Metal-Promoted V_2CO_2 (MXenes): A New and Highly Active Catalyst for Hydrogen Evolution Reaction, *Adv. Sci.*, 2016, **3**, 1600180–1600186.

30 Y. Wang, H. Dou, J. Wang, B. Ding, Y. Xu, Z. Chang and X. Hao, Three-dimensional porous MXene/layered double hydroxide composite for high performance supercapacitors, *J. Power Sources*, 2016, **327**, 221–228.

31 F. Alimohammadi, M. sharifian Gh., N. H. Attanayake, A. C. Thenuwara, Y. Gogotsi, B. Anasori and D. R. Strongin, Antimicrobial Properties of 2D MnO_2 and MoS_2 Nanomaterials Vertically Alined on Graphene Materials and Ti_3C_2 MXene, *Langmuir*, 2018, **34**, 7192–7200.

32 A. M. Jastrzębska, A. Derecka, E. Karwowska, A. Pląsek, T. Wojciechowski, W. Ziemkowska and A. Olszyna, Comparative Assessment of Biocidal Activity of Different RGO/Ceramic Oxide-Ag Nanocomposites, *J. Nano Res.*, 2017, **47**, 89–95.

33 A. M. Jastrzębska, J. Karcz, E. Karwowska, A. Fiedorczuk and A. Olszyna, Synthesis and Bioactivity of Reduced Graphene Oxide/Alumina-Noble Metal Nanocomposite Flakes, *Int. J. Appl. Ceram. Technol.*, 2016, **5**, 856–870.

34 A. M. Jastrzębska, E. Karwowska, P. Kurtycz, E. Miaśkiewicz-Pęska, D. Basiak, A. Olszyna, M. Załęska-Radziwiłł and N. Doskocz, The impact of zeta potential and physicochemical properties of TiO_2-based nanocomposites on their biological activity, *Int. J. Appl. Ceram. Technol.*, 2015, **6**, 1157–1173.

35 A. M. Jastrzębska, A. Szuplewska, T. Wojciechowski, M. Chudy, W. Ziemkowska, L. Chlubny, A. Rozmysłowska and A. Olszyna, *In vitro* studies on cytotoxicity of delaminated Ti_3C_2 MXene, *J. Hazard. Mater.*, 2017, **339**, 1–8, DOI: 10.1016/j.jhazmat.2017.06.004.

36 W. Ziemkowska, D. Basiak, P. Kurtycz, A. Jastrzębska, A. Olszyna and A. Kunicki, Nano-titanium oxide doped with gold, silver and palladium – synthesis and structural characterization, *Chem. Pap.*, 2014, **68**, 959–968.

37 A. M. Jastrzębska, J. Karcz, R. Letmanowski, D. Zabost, E. Ciecierska, J. Zdunek, E. Karwowska, M. Siekierski, A. Olszyna and A. Kunicki, Synthesis of the RGO/Al$_2$O$_3$ core-shell nanocomposite flakes and characterization of their unique electrostatic properties using zeta potential measurements, *Appl. Surf. Sci.*, 2016, **326**, 577–594, DOI: 10.1016/j.apsusc.2015.10.125.

38 A. M. Jastrzębska, J. Jureczko, A. R. Kunicki and A. R. Olszyna, New reduced graphene oxide/alumina (RGO/Al$_2$O$_3$) nanocomposite: innovative method of synthesis and characterization, *Int. J. Appl. Ceram. Technol.*, 2015, **12**, 522–528.

39 A. A. Shamsabadi, M. Sharifian Gh., B. Anasori and M. Soroush, Antimicrobial Mode-of-Action of Colloidal Ti$_3$C$_2$T$_x$ MXene, *ACS Sustainable Chem. Eng.*, 2018, **6**, 16586–16596.

40 A. M. Jastrzębska, J. Karcz, E. Karwowska, A. Fiedorczuk and A. Olszyna, Synthesis and Bioactivity of RGO/TiO$_2$-Noble Metal Nanocomposite Flakes, *J. Nano Res.*, 2017, **47**, 33–48.

41 A. M. Jastrzębska, J. Karcz, E. Karwowska, A. Fiedorczuk and A. Olszyna, Biological properties of the RGO/Al$_2$O$_3$ nanocomposite flakes modified with Ag, Au and Pd for water purification, *J. Alloys Compd.*, 2017, **724**, 869–878.

42 A. M. Jastrzębska, J. Karcz, R. Letmanowski, D. Zabost, E. Ciecierska, M. Siekierski and A. Olszyna, Synthesis of RGO/TiO$_2$ nanocomposite flakes and characterization of their unique electrostatic properties using zeta potential measurements, *J. Alloys Compd.*, 2016, **679**, 470–484.

43 W.-T. Liu, Nanoparticles and their biological and environmental applications, *J. Biosci. Bioeng.*, 2006, **102**, 1–7.

44 A. Kahru, A. Ivask, I. Blinova and H. C. Dubourguier, Bioavailability and ecotoxicology of nanoparticles, *Toxicol. Lett.*, 2008, **180S**, S20.

45 V. Aruoja, H.-C. Dubourguier, K. Kasemets and A. Kahru, Toxicity of ZnO, TiO$_2$ and CuO nanoparticles to microalgae *Pseudokirchneriella subcapitata*, *Toxicol. Lett.*, 2008, **180S**, S220.

46 E. Karwowska, M. Mrozowicz, A. Zawada, T. Ząbkowski, W. Ziemkowska, A. R Kunicki and A. Olszyna, Impact of Al$_2$O$_3$ nanopowders characterized by various physicochemical properties on growth of green alga *Scenedesmus quadricauda*, *Adv. Appl. Ceram.*, 2012, **111**, 142–148.

47 R. J. Miller, H. S. Lenihan, E. B. Muller, N. Tseng, S. K. Hanna and A. A. Keller, Impacts of metal oxide nanoparticles on marine phytoplankton, *Environ. Sci. Technol.*, 2010, **44**, 7329–7334.

48 D. H. Lin and B. S. Xing, Root uptake and phytotoxicity of ZnO nanoparticles, *Environ. Sci. Technol.*, 2008, **42**, 5580–5585.

49 C. C. Chusuei, C. H. Wu, S. Mallavarapu, F. Y. Hou, C. M. Hsu, J. G. Winiarz, R. S. Aronstam and Y. W. Huang, Cytotoxicity in the age of nano: the role of fourth period transition metal oxide nanoparticle physicochemical properties, *Chem.-Biol. Interact.*, 2013, **206**, 319–326.

50 J. H. Lee, J. E. Ju, B. I. Kim, P. J. Pak, E. K. Choi, H. S. Lee and N. Chung, Rod-shaped iron oxide nanoparticles are more toxic than sphere-shaped nanoparticles to murine macrophage cells, *Environ. Toxicol. Chem.*, 2014, **33**, 2759–2766.

51 V. Forest, L. Leclerc, J. F. Hochepie, A. Trouvé, G. Sarry and J. Pourchez, Impact of Cerium Oxide Nanoparticles Shape on their *In Vitro* Cellular Toxicity, *Toxicol. In Vitro*, 2017, **38**, 136–141.

52 M. P. Delorme, Y. Muro, T. Arai, D. A. Banas, S. R. Frame, K. L. Reed and D. B. Warheit, Ninety-day inhalation toxicity study with a vapor grown carbon nanofiber in rats, *Toxicol. Sci.*, 2012, **128**, 449–460.

53 K. Miazek, W. Iwanek, C. Remacle, A. Richel and D. Goffin, Effect of Metals, Metalloids and Metallic Nanoparticles on Microalgae Growth and Industrial product Biosynthesis: A Review, *Int. J. Mol. Sci.*, 2015, **16**, 23929–23969.

54 H. J. Wang, A. C. Growcock, T. H. Tang, J. O'Hara, Y. W. Huang and R. S. Aronstam, Zinc oxide nanoparticle disruption of store-operated calcium entry in a muscarinic receptor signaling pathway, *Toxicol. In Vitro*, 2010, **24**, 1953–1961.

55 T. H. Tang, C. T. Chang, H. J. Wang, J. D. Erickson, R. A. Reichard, A. G. Martin, E. K. Shannon, A. L. Martin, Y. W. Huang and R. S. Aronstam, Oxidative stress disruption of receptor-mediated calcium signaling mechanisms, *J. Biomed. Sci.*, 2013, **20**, 48.

56 X. Lai, Y. Wei, H. Zhao, S. Chen, X. Bu, F. Lu, D. Qu, L. Yao, J. Zheng and J. Zhang, The effect of Fe$_2$O$_3$ and ZnO nanoparticles on cytotoxicity and glucose metabolism in lung epithelial cells, *J. Appl. Toxicol.*, 2015, **35**, 651–664.

57 V. S. Periasamy, J. Athinarayanan, A. Alhazmi, K. A. Alatiah and A. A. Alshatwi, Fe$_3$O$_4$ nanoparticle redox system modulation *via* cell-cycle progression and gene expression in human mesenchymal stem cells, *Environ. Toxicol.*, 2016, **31**, 901–912.

58 Y.-W. Huang, M. Cambre and H.-J. Lee, The Toxicity of Nanoparticles Depends on Multiple Molecular and Physicochemical Mechanisms, *Int. J. Mol. Sci.*, 2017, **18**, 2702, DOI: 10.3390/ijms18122702.

59 R. D. Handy, R. Owen and E. Valsami-Jones, The ecotoxicology of nanoparticles and nanomaterials: current status, knowledge gaps, challenges, an future needs, *Ecotoxicology*, 2008, **17**, 315–325.

60 E. Navarro, A. Baun, R. Behra, N. B. Hartmann, J. Filser, A. J. Miao, A. Quigg, P. H. Santschi and L. Sigg, Environmental behavior and ecotoxicology of engineered nanoparticles to algae, plants and fungi, *Ecotoxicology*, 2008, **17**, 372–386.